Chapter 1
The Finite Element Immersed Boundary Method for the Numerical Simulation of the Motion of Red Blood Cells in Microfluidic Flows

Ronald H.W. Hoppe and Christopher Linsenmann

Abstract We study the mathematical modeling and numerical simulation of the motion of red blood cells (RBCs) subject to an external incompressible flow in a microchannel. RBCs are viscoelastic bodies consisting of a deformable elastic membrane enclosing an incompressible fluid. We study two versions of the Finite Element Immersed Boundary Method (FE-IB), a semi-explicit scheme that requires a CFL-type stability condition and a fully implicit scheme that is unconditionally stable and numerically realized by a predictor-corrector continuation strategy featuring an adaptive choice of the time step sizes. The performance of the two schemes is illustrated by numerical simulations for various scenarios including the tank treading motion in microchannels and the motion through thin capillaries.

Keywords Microfluidic flows · Red blood cells · Finite element immersed boundary method · Semi-explicit scheme · Fully implicit scheme

1.1 Introduction

Red blood cells are viscoelastic bodies which, roughly speaking, consist of a membrane enclosing a liquid [2, 6–9, 26, 30, 31]. When exposed to an external flow, the motion in the fluid represents a fluid-structure interaction problem that can be appropriately modeled by the finite element immersed boundary method (FE-IB). As opposed to the classical immersed boundary method (IB) [24, 25], which is based on a finite difference approach, the FE-IB relies on the variational formulation of the problem [3, 4]. We consider a semi-discretization in space by using Taylor–Hood

R.H.W. Hoppe (✉) · C. Linsenmann
Institute of Mathematics, Universität Augsburg, 86159 Augsburg, Germany
e-mail: hoppe@math.uni-augsburg.de

C. Linsenmann
e-mail: christopher.linsenmann@math.uni-augsburg.de

R.H.W. Hoppe
Department of Mathematics, University of Houston, Houston, TX 77204-3008, USA
e-mail: rohop@math.uh.edu

S. Repin et al. (eds.), *Numerical Methods for Differential Equations, Optimization, and Technological Problems*, Computational Methods in Applied Sciences 27,
DOI 10.1007/978-94-007-5288-7_1,

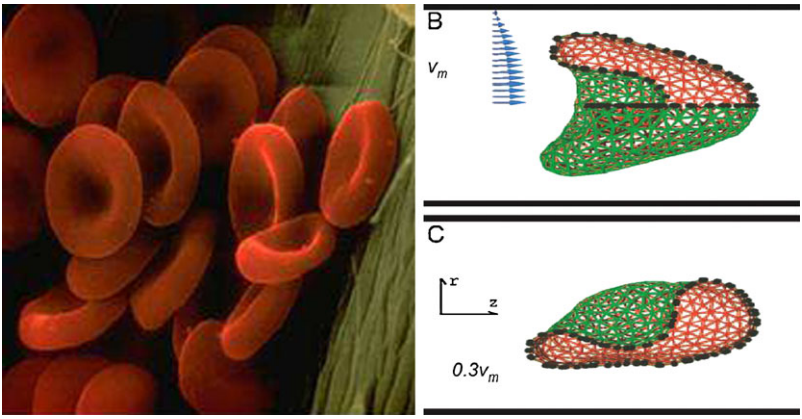

Fig. 1.1 Equilibrium configuration of RBCs (*left*) and deformed shapes in Poiseuille flow (*right*)

P2–P1 elements for the incompressible Navier–Stokes equations and periodic cubic splines for the immersed boundaries. For discretization in time we distinguish between the semi-explicit Backward Euler/Forward Euler FE-IB and the fully implicit Backward Euler/Backward Euler FE-IB where in both cases we use implicit time-stepping for the semi-discretized Navier–Stokes equations. On the other hand, the IB equations are discretized by the forward Euler method in the BE/FE FE-IB and by the backward Euler method in the fully implicit BE/BE FE-IB. The BE/FE FE-IB is subject to a CFL-type condition, whereas the BE/BE FE-IB is unconditionally stable. The latter one will be solved by a predictor-corrector continuation strategy featuring an adaptive choice of the continuation parameter. For both schemes we provide a documentation of numerical results including a comparison with experimental data.

1.2 The Finite Element Immersed Boundary Method

As is well-known, human blood is a suspension of viscoelastic cells, the red and white blood cells, in a viscous fluid, the plasma. The blood flow is not only controlled by the viscosity of the plasma, but additionally viscoelastic effects due to the deformability of the cells, aggregation of the cells, and hematocrit come into play and have been experimentally observed.

If not being subjected to an external flow, red blood cells (RBCs) are biconcavely shaped disks with a diameter of 7.5–8.0 μm and a thickness of about 2 μm (cf. Fig. 1.1 (left)). However, under the influence of an external flow, the cells deform and may attain parachute- or slipper-like shapes in Poiseuille flow depending on their position (centered or decentered) in the flow field [22] (cf. Fig. 1.1 (right)).

The FE-IB describes the fluid-structure interaction problem based on a coupled Eulerian/Lagrangian approach. The external fluid flow is modeled by the incompressible Navier–Stokes equations in an Eulerian coordinate system, whereas the

boundaries of the immersed bodies are described by means of a Lagrangian coordinate system. For its variational formulation, we will use standard notation from Lebesgue and Sobolev space theory [29].

In particular, we assume the computational domain $\Omega := (a,b) \times (c,d)$, $a < b$, $c < d$, to be a microchannel with boundary $\Gamma := \bar{\Gamma}_{\text{in}} \cup \bar{\Gamma}_{\text{out}} \cup \bar{\Gamma}_{\text{lat}}$, where $\Gamma_{\text{in}} := \{a\} \times (c,d)$, $\Gamma_{\text{out}} := \{b\} \times (c,d)$, and $\Gamma_{\text{lat}} := (a,b) \times \{c\} \cup (a,b) \times \{d\}$. We further assume a stationary velocity g at the inflow boundary Γ_{in} and the outflow boundary Γ_{out} as well as zero velocity at the lateral boundary Γ_{lat}. The impact of the immersed bodies on the external force is described by a force density $\mathbf{F}$ which will be specified later. Denoting by ρ, μ the density and the viscosity of the external fluid, by $\mathbf{u}$, p the velocity and the pressure, by $\mathbf{u}^{(0)}$ an initial velocity, and by $\mathbf{n}_{\Sigma_{\text{in}}}$, $\mathbf{n}_{\Sigma_{\text{out}}}$, $\mathbf{t}_{\Sigma_{\text{in}}}$, $\mathbf{t}_{\Sigma_{\text{out}}}$ the exterior unit normal vectors and unit tangential vectors on Σ_{in}, Σ_{out}, the incompressible Navier–Stokes equations read

$$\rho\left(\frac{\partial \mathbf{v}}{\partial t} + (\mathbf{u}\cdot\nabla)\mathbf{v}\right) - \mu\Delta\mathbf{u} + \nabla p = \mathbf{F} \qquad \text{in } Q := \Omega \times (0,T], \tag{1.1a}$$

$$\nabla\cdot\mathbf{u} = 0 \qquad \text{in } Q, \tag{1.1b}$$

$$\mathbf{t}_{\Sigma_{\text{in}}}\cdot\mathbf{u} = 0, \quad \mathbf{n}_{\Sigma_{\text{in}}}\cdot\mathbf{u} = g \qquad \text{on } \Sigma_{\text{in}} := \Gamma_{\text{in}} \times (0,T], \tag{1.1c}$$

$$\mathbf{t}_{\Sigma_{\text{out}}}\cdot\mathbf{u} = 0, \quad \mathbf{n}_{\Sigma_{\text{out}}}\cdot\mathbf{u} = g \qquad \text{on } \Sigma_{\text{out}} := \Gamma_{\text{out}} \times (0,T], \tag{1.1d}$$

$$\mathbf{u} = 0 \qquad \text{on } \Sigma_{\text{lat}} := \Gamma_{\text{lat}} \times (0,T], \tag{1.1e}$$

$$\mathbf{u}(\cdot,0) = \mathbf{u}^{(0)} \qquad \text{in } \Omega. \tag{1.1f}$$

The boundary of an immersed body is supposed to be a smooth closed and non-intersecting, massless curve of length L driven by the velocity $\mathbf{u}$. Denoting by $\mathbf{X}$ the position vector of the boundary, by $\mathbf{X}^{(0)}$ the initial configuration, and assuming periodic boundary conditions, the equations of motion of the immersed body read

$$\frac{\partial \mathbf{X}}{\partial t} = \mathbf{u}\big(\mathbf{X}(\cdot,t),t\big), \tag{1.2a}$$

$$\mathbf{X}(q,0) = \mathbf{X}^{(0)}(q), \qquad q \in [0,L], \tag{1.2b}$$

$$\partial^k\mathbf{X}/\partial q^k(0,t) = \partial^k\mathbf{X}/\partial q^k(L,t), \quad k = 0,1,2. \tag{1.2c}$$

The force density $\mathbf{F} \in \mathbf{L}^2((0,T),\mathbf{H}^{-1}(\Omega))$ in (1.1a) is given by

$$\big\langle \mathbf{F}(t),\mathbf{v}\big\rangle = \int_0^L \mathbf{f}(q,t)\cdot\mathbf{v}\big(\mathbf{X}(q,t)\big)\,dq \quad \text{for almost all } t \in (0,T). \tag{1.3}$$

Here, $\langle\cdot,\cdot\rangle$ stands for the dual pairing between $\mathbf{H}^{-1}(\Omega)$ and $\mathbf{H}_0^1(\Omega)$. The local force density $\mathbf{f}$ is defined according to $\mathbf{f}(q,t) = -E'(\mathbf{X}(q,t))$ by means of the Gâteaux derivative E' of the total energy $E(t) := E^e(t) + E^b(t)$, where

$$E^e(t) := \int_0^L \frac{\kappa_e}{2}\left(\left|\frac{\partial \mathbf{X}}{\partial q}(q,t)\right| - 1\right)^2 dq, \tag{1.4a}$$

$$E^b(t) := \int_0^L \frac{\kappa_b}{2} \left| \frac{\partial^2 \mathbf{X}}{\partial q^2}(q,t) \right|^2 dq. \tag{1.4b}$$

We introduce the function spaces

$$\begin{aligned}
\mathbf{V}(0,T) &:= \mathbf{H}^1\big((0,T), \mathbf{H}^{-1}(\Omega)\big) \cap \mathbf{L}^2\big((0,T), \mathbf{H}^1(\Omega)\big),\\
\mathbf{W}(0,T) &:= \big\{\mathbf{w} \in \mathbf{V}(0,T) \mid \mathbf{n}_{\Sigma_{\text{in}}} \cdot \mathbf{w}|_{\Sigma_{\text{in}}} = \mathbf{n}_{\Sigma_{\text{out}}} \cdot \mathbf{w}|_{\Sigma_{\text{out}}} = g,\\
&\qquad \mathbf{t}_{\Sigma_{\text{in}}} \cdot \mathbf{w}|_{\Sigma_{\text{in}}} = \mathbf{t}_{\Sigma_{\text{out}}} \cdot \mathbf{w}|_{\Sigma_{\text{out}}} = 0,\ \mathbf{w}|_{\Sigma_{\text{lat}}} = 0\big\},\\
\mathbf{W}_0(0,T) &:= \big\{\mathbf{w} \in \mathbf{V}(0,T) \mid \mathbf{w}_{\Gamma \times (0,T]} = \mathbf{0}\big\},\\
Q(0,T) &:= L^2\big((0,T), L_0^2(\Omega)\big).
\end{aligned}$$

The variational formulation of the FE-IB amounts to the computation of

$$(\mathbf{u}, p, \mathbf{X}) \in \mathbf{W}(0,T) \times Q(0,T) \times \mathbf{H}^1\big((0,T), \mathbf{L}^2\big([0,L]\big)\big) \cap \mathbf{L}^2\big((0,T), \mathbf{H}^3_{per}\big([0,L]\big)\big)$$

such that for all $(\mathbf{w}, q) \in \mathbf{W}_0(0,T) \times Q(0,T)$ there holds

$$\left\langle \rho \frac{\partial \mathbf{u}}{\partial t}, \mathbf{w} \right\rangle + a(\mathbf{u}, \mathbf{w}) - b(p, \mathbf{w}) = \big\langle \mathbf{F}(t), \mathbf{w} \big\rangle, \tag{1.5a}$$

$$b(q, \mathbf{u}) = 0, \tag{1.5b}$$

$$\mathbf{u}(\cdot, 0) = \mathbf{u}^{(0)}, \tag{1.5c}$$

and $\mathbf{X}$ satisfies (1.2a)–(1.2c). Here, the forms $a(\cdot,\cdot)$ and $b(\cdot,\cdot)$ are given by

$$a(\mathbf{u}, \mathbf{v}) := \big(\rho(\mathbf{u} \cdot \nabla)\mathbf{u}, \mathbf{v}\big)_{0,\Omega} + (\mu \nabla \mathbf{u}, \nabla \mathbf{v})_{0,\Omega}, \tag{1.6a}$$

$$b(p, \mathbf{v}) := (p, \nabla \cdot \mathbf{v})_{0,\Omega}. \tag{1.6b}$$

The following result provides an energy estimate for the FE-IB.

Theorem 1 *Suppose that the data of the FE-IB satisfy*

$$\mathbf{F} \in \mathbf{L}^2\big((0,T); \mathbf{H}^{-1}(\Omega)\big), \qquad \mathbf{u}^{(0)} \in \mathbf{L}^2(\Omega), \tag{1.7a}$$

$$g \in H_{00}^{5/2+s}(\Gamma_{\text{in}} \cup \Gamma_{\text{out}}), \qquad s \in (0, 1/2), \tag{1.7b}$$

and

$$\|g\|_{H_{00}^{5/2+s}(\Gamma_{\text{in}})} \le \big(4\rho C(\Omega)\big)^{-1} \mu, \quad s \in (0, 1/2), \tag{1.8}$$

for some constant $C(\Omega) > 0$, depending on the domain Ω. Then, if the triple $(\mathbf{u}, p, \mathbf{X})$ solves (1.5a)–(1.5c) and (1.2a)–(1.2c), there exist positive constants C_i, $1 \le i \le 2$, only depending on the data of the problem, and $C(g)$, only depending

on g, such that

$$\frac{\rho}{4}\left\|\mathbf{u}(\cdot,t)\right\|_{0,\Omega}^2+\frac{\mu}{4}\int_0^t\left\|\nabla\mathbf{u}(\cdot,\tau)\right\|_{0,\Omega}^2 d\tau+E(t)$$
$$\leq C_1\left(1+C_2\,t\;+\left\|\mathbf{u}^{(0)}\right\|_{0,\Omega}^2+E(0)+C(g)\int_0^t E(\tau)\,d\tau\right).$$

Proof We refer to [14]. □

1.3 Space/Time Discretization

For the spatial discretization of the incompressible Navier–Stokes equations we use P2–P1 Taylor–Hood elements [5] with respect to a simplicial triangulation $\mathscr{T}_h(\Omega)$ of the computational domain Ω. For $T\in\mathscr{T}_h(\Omega)$, we refer to h_T as the diameter of T and set $h:=\max_{T\in\mathscr{T}_h(\Omega)}h_T$. We further denote by $P_k(T)$, $k\in\mathbb{N}$, the linear space of polynomials of degree $\leq k$ on T, and we choose the function spaces

$$\mathbf{V}_h:=\left\{\mathbf{v}_h\in C(\bar{\Omega})^2\mid v_h|_T\in P_2(T)^2\right\},\qquad Q_h:=\left\{q_h\in C(\bar{\Omega})\mid q_h|_T\in P_1(T)\right\},$$

and

$$\begin{aligned}\mathbf{W}_h(0,T):=\big\{&\mathbf{w}_h\in C\big([0,T],C(\bar{\Omega})^2\big)\mid\mathbf{w}_h(\cdot,t)\in\mathbf{V}_h,\\&\mathbf{n}_{\Gamma_{\text{in}}}\cdot\mathbf{w}_h=\mathbf{n}_{\Gamma_{\text{out}}}\cdot\mathbf{w}_h=g_h,\\&\mathbf{t}_{\Gamma_{\text{in}}}\cdot\mathbf{w}_h=\mathbf{t}_{\Gamma_{\text{out}}}\cdot\mathbf{w}_h=0,\;\mathbf{n}_{\Gamma_{\text{lat}}}\cdot\mathbf{w}_h=0\big\},\\\mathbf{W}_{h,0}(0,T):=\big\{&\mathbf{w}_h\in\mathbf{W}_h(0,T)\mid\mathbf{w}_h|_{\Gamma\times(0,T)}=0\big\},\\Q_h(0,T):=\big\{&q_h\in C\big([0,T],C(\bar{\Omega})\cap L_0^2(\Omega)\big)\mid q_h(\cdot,t)\in Q_h\big\}.\end{aligned}$$

Given some approximation $g_h\in C([0,T],C^2(\Gamma_{\text{in}}))$ of the inflow velocity g and $\mathbf{u}_h^{(0)}\in\mathbf{V}_h$ of the initial velocity $\mathbf{u}^{(0)}$, we compute $(\mathbf{u}_h,p_h)\in\mathbf{W}_h(0,T)\times Q_h(0,T)$ such that for all $(\mathbf{w}_h,q_h)\in\mathbf{W}_{h,0}(0,T)\times Q_h(0,T)$ and $t\in[0,T]$ there holds

$$\left(\rho\frac{\partial\mathbf{u}_h}{\partial t},\mathbf{w}_h\right)_{0,\Omega}+a(\mathbf{u}_h,\mathbf{w}_h)-b(p_h,\mathbf{w}_h)=\left\langle\mathbf{F}_h(t),\mathbf{w}_h\right\rangle_h,\tag{1.9a}$$

$$b(q_h,\mathbf{u}_h)=0,\tag{1.9b}$$

$$\mathbf{u}_h(0,t)=\mathbf{u}_h^{(0)},\tag{1.9c}$$

where $\langle\mathbf{F}_h(t),\mathbf{w}_h\rangle_h$ will be defined by (1.11) below.

We discretize the immersed boundary by periodic cubic splines with respect to a partition

$$\mathscr{T}_{[0,L]}:=\{0=:q_0<q_1<\cdots<q_M:=L\},\quad M\in\mathbb{N},$$

of the interval $[0, L]$ into subintervals $I_i := [q_{i-1}, q_i]$ of length $\Delta q_i := q_i - q_{i-1}$, and we set

$$\mathbf{S}_h := \big\{\mathbf{Y}_h \in C^2\big([0, L], \Omega\big) \mid \mathbf{Y}_h|_{I_i} \in P_3(I_i)^2,\ \mathbf{Y}_h^{(k)}(q_0) = \mathbf{Y}_h^{(k)}(q_M),\ 0 \le k \le 2\big\}.$$

Given some approximation $\mathbf{X}_h^{(0)} \in \mathbf{S}_h$ of $\mathbf{X}^{(0)}$, we look for $\mathbf{X}_h \in C^1([0, T], \mathbf{S}_h)$ such that

$$\frac{\partial \mathbf{X}_h}{\partial t} = \mathbf{u}_h\big(\mathbf{X}_h(\cdot, t), t\big), \quad 0 < t \le T, \tag{1.10a}$$

$$\mathbf{X}_h(\cdot, 0) = \mathbf{X}_h^{(0)}. \tag{1.10b}$$

Finally, the right-hand side in (1.9a) reads as follows:

$$\begin{aligned}\big\langle \mathbf{F}_h(t), \mathbf{w}_h\big\rangle_h = &-\kappa_e \int_0^L \frac{\partial \mathbf{X}_h}{\partial q} \cdot \nabla \mathbf{w}_h\big(\mathbf{X}_h(q, t)\big)\, \frac{\partial \mathbf{X}_h}{\partial q}\, dq \\ &+ \kappa_b \sum_{i=1}^M \frac{\partial^3 \mathbf{X}_h}{\partial q^3}\bigg|_{I_i} \cdot \int_{q_{i-1}}^{q_i} \nabla \mathbf{w}_h\big(\mathbf{X}_h(q, t)\big) \frac{\partial \mathbf{X}_h}{\partial q}\, dq. \end{aligned} \tag{1.11}$$

For discretization in time, we consider a partition $\mathcal{T}_{[0,T]}$ of the time interval $[0, T]$

$$\mathcal{T}_{[0,T]} := \{0 =: t_0 < t_1 < \cdots < t_N := T\}, \quad N \in \mathbb{N},$$

into subintervals $[t_n, t_{n+1}]$, $0 \le n \le N-1$, of length $\tau_n := t_{n+1} - t_n$. We denote by $\mathbf{u}_h^{(n)}$ approximations of $\mathbf{u}_h$ at times t_n and define

$$D_{\Delta t}^+ \mathbf{u}_h^{(n)} := \frac{\mathbf{u}_h^{(n+1)} - \mathbf{u}_h^{(n)}}{\Delta \tau_n}.$$

Semi-explicit Scheme The Backward Euler/Forward Euler FE-IB (BE/FE FE-IB) is a semi-explicit scheme where we discretize the semi-discrete Navier–Stokes equations (1.9a)–(1.9c) by the implicit Euler scheme and the immersed boundary equations (1.10a), (1.10b) by the explicit Euler scheme. In particular, given $\mathbf{u}_h^{(0)}$, for $n \ge 0$ we first compute $(\mathbf{u}_h^{(n+1)}, p_h^{(n+1)}) \in \mathbf{V}_h \times Q_h$ such that

$$\big(\rho\ D_{\Delta t}^+ \mathbf{u}_h^{(n)}, \mathbf{w}_h\big)_{0,\Omega} + a\big(\mathbf{u}_h^{(n+1)}, \mathbf{w}_h\big) - b\big(p_h^{(n+1)}, \mathbf{w}_h\big) = \big\langle \mathbf{F}_h^{(n)}, \mathbf{w}_h\big\rangle_h, \tag{1.12a}$$

$$b\big(q_h, \mathbf{u}_h^{(n+1)}\big) = 0, \tag{1.12b}$$

where

$$\langle \mathbf{F}_h^{(n)}, \mathbf{w}_h \rangle_h := -\kappa_e \int_0^L \frac{\partial \mathbf{X}_h^{(n)}}{\partial q} \cdot \frac{\partial}{\partial q} \mathbf{w}_h\big(\mathbf{X}_h^{(n)}\big)\, dq + \kappa_b \sum_{i=1}^{M} \left. \frac{\partial^3 \mathbf{X}_h^{(n)}}{\partial q^3} \right|_{I_i} \cdot \int_{q_{i-1}}^{q_i} \frac{\partial}{\partial q} \mathbf{w}_h\big(\mathbf{X}_h^{(n)}\big)\, dq$$

and then compute $\mathbf{X}_h^{(n+1)} \in \mathbf{S}_h$ according to

$$\int_0^L \mathbf{X}_h^{(n+1)} \cdot \mathbf{Y}_h\, dq = \tau_n \int_0^L \mathbf{u}_h^{(n)}\big(\mathbf{X}_h^{(n)}\big) \cdot \mathbf{Y}_h\, dq + \int_0^L \mathbf{X}_h^{(n)} \cdot \mathbf{Y}_h\, dq, \quad \mathbf{Y}_h \in \mathbf{S}_h. \tag{1.13}$$

In case of an equidistant partition $\mathscr{T}_{[0,T]}$ with $\tau_n = \Delta t := T/N$, the following stability estimate holds true (cf. [14]).

Theorem 2 *In addition to the assumptions of Theorem 1 suppose that the CFL-type condition*

$$\frac{\Delta \tau}{h} \le \frac{\mu}{4 C_B (\kappa_e L_1 + \kappa_b L_2)}, \tag{1.14}$$

is satisfied, where $C_B > 0$ is a computable constant, depending on the domain Ω, and the constants L_i, $1 \le i \le 2$, are given by

$$\begin{aligned} L_1 &:= \max_{0 \le n \le N} \max_{q \in [0,L]} \big|\partial \mathbf{X}_h^{(n)} / \partial q\big|, \\ L_2 &:= \max_{0 \le n \le N} \max_{1 \le i \le M} \max_{q \in I_i} \big|\partial^3 \mathbf{X}_h^{(n)} / \partial q^3 |_{I_i}\big|. \end{aligned} \tag{1.15}$$

Then, if $(\mathbf{u}_h, p_h, \mathbf{X}_h)$ solves the BE/FE FE-IB (1.12a), (1.12b), (1.13), there exist positive constants C_i, $4 \le i \le 6$, depending only on the data of the problem, such that

$$\begin{aligned} &\frac{\rho}{4} \big\|\mathbf{u}_h^{(n)}\big\|_{0,\Omega}^2 + \frac{\mu}{4} \sum_{m=1}^{n} \big\|\nabla \mathbf{u}_h^{(m)}\big\|_{0,\Omega}^2 \Delta \tau + E_h^{(n)} \\ &\quad \le C_4 \left(1 + C_5\, t_n + \big\|\mathbf{u}_h^{(0)}\big\|_{0,\Omega}^2 + E_h^{(0)} + C_6 \sum_{m=1}^{n-1} E_h^{(m)} \Delta \tau \right). \end{aligned} \tag{1.16}$$

Remark 1 Semi-explicit schemes based on the classical IB have been applied to the simulation of the motion of RBCs in [11, 23, 33].

Fully Implicit Scheme The Backward Euler/Backward Euler FE-IB (BE/BE FE-IB) is a fully implicit scheme where we discretize both the semi-discrete Navier–Stokes equations (1.9a)–(1.9c) and the immersed boundary equations (1.10a),

(1.10b) by the backward Euler scheme. In particular, we simultaneously compute $(\mathbf{u}_h^{(n+1)}, p_h^{(n+1)}) \in \mathbf{V}_h \times Q_h$ such that for all $\mathbf{w}_h \in \mathbf{W}_{h,0}(0,T)$, $q_h \in Q_h$ it holds

$$\big(\rho\, D_{\tau_n}^{+}\mathbf{u}_h^{(n)}, \mathbf{w}_h\big)_{0,\Omega} + a\big(\mathbf{u}_h^{(n+1)}, \mathbf{w}_h\big) - b\big(p_h^{(n+1}, \mathbf{w}_h\big) = \big\langle \mathbf{F}_h^{(n+1)}, \mathbf{w}_h\big\rangle_h, \tag{1.17a}$$

$$b\big(q_h, \mathbf{u}_h^{(n+1)}\big) = 0, \tag{1.17b}$$

where

$$\begin{aligned}\big\langle \mathbf{F}_h^{(n+1)}, \mathbf{w}_h\big\rangle_h := &-\kappa_e \int_0^L \frac{\partial \mathbf{X}_h^{(n+1)}}{\partial q} \cdot D^1\mathbf{w}_h\big(\mathbf{X}_h^{(n+1)}\big)\frac{\partial \mathbf{X}_h^{(n+1)}}{\partial q}\, dq \\ &+ \kappa_b \int_0^L \frac{\partial^2 \mathbf{X}_h^{(n+1)}}{\partial q^2} \cdot \bigg(D^1\mathbf{w}_h\big(\mathbf{X}_h^{(n+1)}\big)\frac{\partial^2 \mathbf{X}_h^{(n+1)}}{\partial q^2} \\ &+ D^2\mathbf{w}_h\big(\mathbf{X}_h^{(n+1)}\big)\bigg(\frac{\partial \mathbf{X}_h^{(n+1)}}{\partial q}, \frac{\partial \mathbf{X}_h^{(n+1)}}{\partial q}\bigg)\bigg)\, dq,\end{aligned}$$

and compute $\mathbf{X}_h^{(n+1)} \in \mathbf{S}_h$ such that for all $\mathbf{Y}_h \in \mathbf{S}_h$ there holds

$$\int_0^L \mathbf{X}_h^{(n+1)} \cdot \mathbf{Y}_h\, dq - \tau_n \int_0^L \mathbf{u}_h^{(n+1)}\big(\mathbf{X}_h^{(n+1)}\big) \cdot \mathbf{Y}_h\, dq = \int_0^L \mathbf{X}_h^{(n)} \cdot \mathbf{Y}_h\, dq. \tag{1.18}$$

Remark 2 For the classical IB, semi-explicit, approximate implicit, and fully implicit schemes have been considered in [18–21, 28], whereas the unconditional stability of fully implicit FE-IB methods has been shown in [4].

1.4 Predictor–Corrector Continuation Strategy for the Numerical Solution of the Fully Implicit Scheme

The numerical realization of the fully implicit BE/BE FE-IB amounts to the solution of a nonlinear system of equations. The application of Newton's method turns out to be delicate, since the numerical stiffness of the BE/BE FE-IB significantly affects the convergence radius of Newton's method in a negative way. In compliance with this, for the fully implicit IB it was stated in [32] that Newton's method is computationally too expensive in practice. To overcome this difficulty, we will use a continuation method in a predictor–corrector manner. Thereby, the time increment is chosen adaptively in such a way that the convergence requirements of Newton's method for the next time step are met. Consequently, a successful application of Newton's method is guaranteed without an expensive search for proper initial guesses.

At each time-step, the BE/BE FE-IB (1.17a), (1.17b), (1.18) amounts to the computation of $\mathbf{z}^{(n+1)} := (\mathbf{u}^{(n+1)}, p^{(n+1)}, \mathbf{X}^{(n+1)})^T$, $0 \le n \le M-1$, as the solution of

the parameter dependent nonlinear system

$$\mathbf{G}\big(\mathbf{z}^{(n+1)};\tau_n\big)=0, \tag{1.19}$$

where the nonlinear mapping $\mathbf{G}(\cdot;\tau_n):\mathbb{R}^{\mathcal{N}}\to\mathbb{R}^{\mathcal{N}}$ is given by

$$\mathbf{G}(\mathbf{z};\tau_n)=\begin{pmatrix}(\mathbf{M}_1+\tau_n\mathbf{A})\mathbf{u}+\tau_n\mathbf{C}(\mathbf{u})+\tau_n\mathbf{B}^T p-\tau_n\mathbf{F}(\mathbf{X})-\mathbf{M}_1\mathbf{u}^{(n)}-\tau_n\mathbf{F}_0\\ \mathbf{B}\mathbf{u}-\mathbf{b}\\ \mathbf{M}_3\mathbf{X}-\mathbf{M}_3\mathbf{X}^{(n)}-\tau_n\mathbf{K}(\mathbf{X})\mathbf{u}\end{pmatrix}. \tag{1.20}$$

Here, $\mathbf{M}_1$, $\mathbf{A}$, and $\mathbf{B}$ are the mass and stiffness matrices associated with the fully discretized Navier–Stokes equations (1.17a), (1.17b). $\mathbf{M}_3$ is the mass matrix associated with (1.18). The nonlinear maps $\mathbf{C}(\mathbf{u})$ and $\mathbf{K}(\mathbf{X})$ are associated with the nonlinear parts of (1.17a), (1.18), respectively, and $\mathbf{b}$, $\mathbf{F}_0$ are vectors stemming from the inhomogeneous boundary data on Σ_{in}. For scaling purposes, we have multiplied the second block in (1.20) with τ_n^{-1}.

We note that the continuation parameter is the time t. We attempt to solve (1.19) by a path-following predictor–corrector continuation strategy with constant continuation as a predictor featuring an adaptive choice of the continuation steplength and a Newton-type method as a corrector [10]. A first result in this direction is the invertibility of the Jacobian $\mathbf{G}'(\mathbf{z};\tau_n)$.

Theorem 3 *For given $\mathbf{z}\in\mathbb{R}^{\mathcal{N}}$ and $\tau^{\min}>0$ there exists $\tau_n^{\max}(z)$ such that for all step sizes $\tau^{\min}\le\tau_n\le\tau_n^{\max}$ the Jacobian*

$$\mathbf{G}'(\mathbf{z};\tau_n)=\begin{pmatrix}\mathbf{M}_1+\tau_n\mathbf{A}+\tau_n\mathbf{C}'(\mathbf{u}) & \tau_n\mathbf{B}^T & -\tau_n\mathbf{F}'(\mathbf{X})\\ \mathbf{B} & \mathbf{0} & \mathbf{0}\\ -\tau_n\mathbf{K}(\mathbf{X}) & \mathbf{0} & \mathbf{M}_3-\tau_n\mathbf{K}'_{\mathbf{X}}(\mathbf{X},\mathbf{u})\end{pmatrix} \tag{1.21}$$

is invertible with bounded inverse

$$\big\|\big(\mathbf{G}'(\mathbf{z};\tau_n)\big)^{-1}\big\|\le\Lambda_n,$$

where Λ_n depends on $\tau^{\min}$ and $\tau_n^{\max}(z)$.

Proof For a proof we refer to [15]. □

The adaptive predictor-corrector continuation strategy is as follows:

Initialization Specify the initial variables $\mathbf{z}(t_0)=(\mathbf{u}^{(0)},p^{(0)},\mathbf{X}^{(0)})^T$, an initial continuation step size $\tau_{(0,0)}>0$, and bounds $\tau^{\min}$, $\tau^{\max}$, $\Theta_{\min}\ll 1$. Set $n=j=0$. Here, n is the iteration counter for the outer continuation, whereas j is the iteration counter for the inner predictor–corrector cycles.

Step 1: Predictor As long as $t_n<T$, set $t_{(n+1,j)}:=t_n+\tau_{(n,j)}$ and perform the continuation

$$\hat{\mathbf{z}}^{(0)}(t_{(n+1,j)}):=\mathbf{z}(t_n).$$

Step 2: Corrector Solve $\mathbf{G}(z;\tau_{(n,j)})=0$ by a combination of the ordinary and the simplified Newton method with initial guess $\hat{\mathbf{z}}^{(0)}(t_{(n+1,j)})$ and iteration counter $\ell=\ell(j)\geq 0$. Thereby, $\mathbf{z}$ gets updated by means of

$$\hat{\mathbf{z}}^{(\ell+1)}(t_{(n+1,j)}):=\hat{\mathbf{z}}^{(\ell)}(t_{(n+1,j)})+\alpha_\ell\Delta\mathbf{z}^{(\ell)},$$

where $\alpha_\ell>0$ is a suitable damping factor, and contraction factors Θ_ℓ, $\ell\geq 0$, are computed according to

$$\Theta_\ell:=\frac{\|\overline{\Delta\mathbf{z}}^{\ell+1}\|}{\|\overline{\Delta\mathbf{z}}^{\ell}\|},\quad \ell\geq 0.$$

The contraction factors serve as a convergence monitor in the simplified Newton method. If the simplified Newton corrector was successful, predict the new continuation step size by

$$\tau_{(n+1,0)}:=\min\left(\frac{(\sqrt{2}-1)\|\Delta\mathbf{z}^{(0)}\|}{2\max(\Theta_0,\Theta_{\min})\|\mathbf{z}(t_n)-\mathbf{z}(t_{n+1})\|}\tau_{(n,j)},\tau_{\max}\right),$$

where $t_{n+1}:=t_{(n+1,j)}$ and $\mathbf{z}(t_{n+1}):=\hat{\mathbf{z}}^{(\ell)}(t_{(n+1,j)})$. Set $n:=n+1$, $j:=0$ and go to Step 1.
Else correct the continuation step size τ by means of

$$\tau_{(n,j+1)}:=\frac{(\sqrt{2}-1)}{\sqrt{4\Theta_\ell+1}-1}\tau_{(n,j)}.$$

If $\tau_{(n,j+1)}<\tau_{\min}$, stop the algorithm (convergence failure). Otherwise, set $j:=j+1$ and go to Step 1.

1.5 Documentation of Numerical Results

In this section, we provide a documentation of simulation results for both the semi-explicit BE/FE FE-IB and the fully implicit BE/BE FE-IB.

1.5.1 The Semi-explicit BE/FE FE-IB

For studying the so-called tank treading motion [1, 12, 13, 16, 17] of viscoelastic particles under shear flow, we have applied the semi-explicit BE/FE FE-IB to a microchannel $\Omega=(0.0,1.2)\times(0.0,0.1)10^{-3}$ m with inflow boundary $\Gamma_{\text{in}}=\{0.0\}\times(0.0,0.1)$, inflow velocity $g=1.0\times 10^{-4}$ m/s, and outflow boundary $\Gamma_{\text{out}}:=\{1.2\}\times(0.0,0.1)$. We have further used $\rho=1.0\times 10^3$ kg/m^3 and $\mu=6.0\times 10^{-3}$ Pa/s resulting in a Reynolds number of approximately 0.1 which is

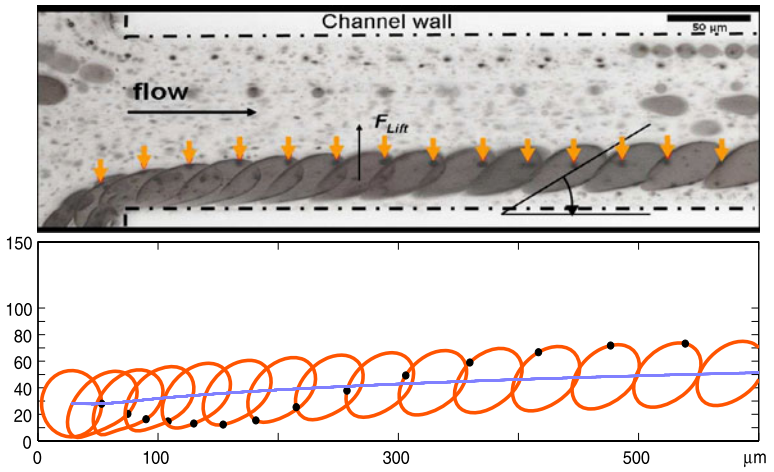

Fig. 1.2 Tank treading motion of a vesicle in shear flow: snapshots from experimental data (*top*) and numerical simulation by the FE/BE FE-IB (*bottom*)

typical for microfluidic flows. The elasticity coefficients have been chosen according to $\kappa_e = 6.0 \times 10^{-6}$ N/m and $\kappa_b = 2.0 \times 10^{-19}$ N/m, which correspond to the values of RBCs [11]. We have chosen a simplicial triangulation with $h = \sqrt{2}/16$ and an equidistant partitioning of $[0, L]$ with $\Delta q = h/2$ giving rise to a total of 42555 degrees of freedom. The time step has been chosen as $\Delta t = 1/240$.

Figure 1.2 displays snapshots from experimental data (top) and the simulation results due to the application of the BE/FE FE-IB (bottom). The initially spherical particle first gets deformed by attaining an ellipsoidal shape and then continues to move forward with a rotating membrane (cf. the motion of a material point on the immersed boundary marked by an arrow in the experimental result and by a black dot in the simulations). As can be observed as well, the particle experiences some lift towards the center of the channel. We computed an inclination angle of 34° which is in very good agreement with the experimental data.

The deformability of RBCs is such that they can pass through capillaries with diameters significantly less than the diameter of an RBC [27]. We have studied the motion of an RBC in a microchannel of width 20×10^{-6} m featuring a capillary of width 4.0×10^{-6} m (cf. Fig. 1.3). The inflow and outflow occur through the left and right boundary of the microchannel, respectively. The inflow velocity g as well as the other data ρ, μ, κ_e, κ_b have been chosen as in the previous example. For discretization in space and time, we have used $h = 1/15$ and $\Delta q = h/2$ yielding a total of 26709 degrees of freedom and a time step size of $\Delta t = 1/1000$. We note that Δt had to be chosen that small in order to satisfy the CFL condition (1.14), since the velocity at the opening of the capillary is almost five times higher than the inflow velocity. Figure 1.3 (top) displays the results obtained by the BE/FE FE-IB. For comparison, Fig. 1.3 (bottom) shows the snapshot of an RBC shortly before leaving a capillary in an experimental set up under essentially the same flow conditions. The

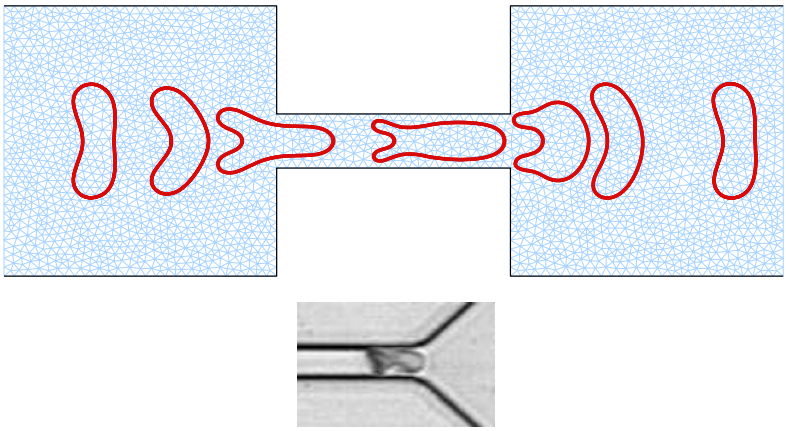

Fig. 1.3 RBC passing through a capillary of half its resting diameter: numerical simulation by the BE/FE FE-IB (*top*) and snapshot from an experiment (*bottom*)

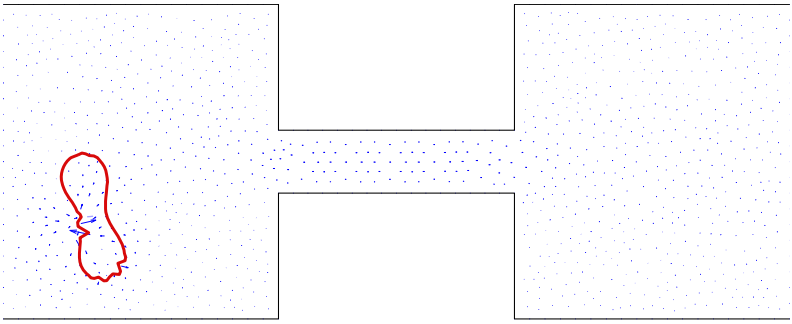

Fig. 1.4 Breakdown of the BE/FE FE-IB for $\tau = 1/250$ due to high oscillations of membrane nodes

fish-like shape of the RBC inside the capillary is very well captured by the numerical simulation.

1.5.2 The Fully Implicit BE/BE FE-IB

The motion of an RBC through a thin capillary is an appropriate example to illustrate the limitations of the semi-explicit BE/FE FE-IB and the advantages of the fully implicit BE/BE FE-IB. We have studied the same scenario as before, but applied the BE/FE FE-IB with a time step size $\Delta t = 1/250$. Figure 1.4 shows the onset of numerical instabilities due to oscillations of membrane nodes which caused a breakdown of the algorithm after $t = 0.05$. Such instabilities do not occur when

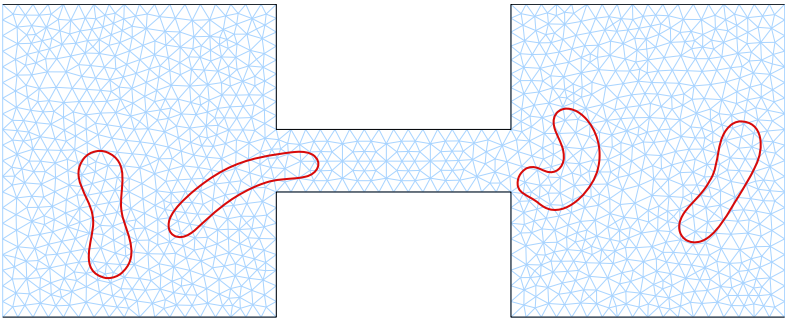

Fig. 1.5 Application of the BE/BE FE-IB: Snapshots of the RBC's membrane at selected time instants corresponding to the $*$-marked time instants in Fig. 1.6

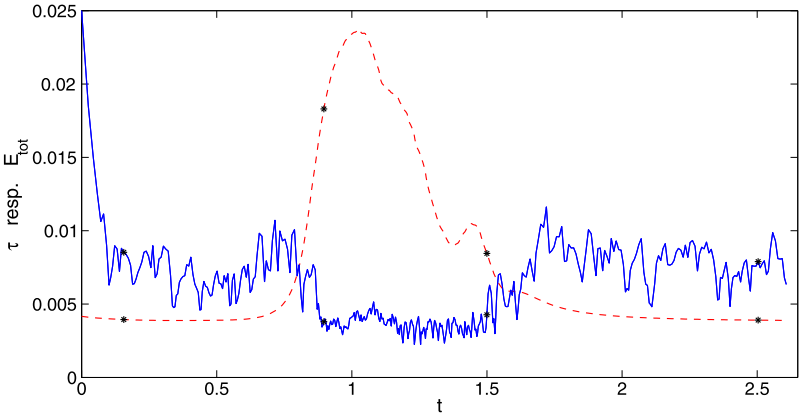

Fig. 1.6 Application of the BE/BE FE-IB: Evolution of the adaptively chosen time step sizes (*solid line*) and of the (*scaled*) total energy (*dashed line*)

using the fully implicit BE/BE FE-IB and its numerical realization by the predictor-corrector continuation strategy as described in Sect. 1.4 (cf. Fig. 1.5).

In fact, the adaptive time step size selection detects the critical stage of the process which occurs when the RBC starts to deform before entering the capillary and thus leads to a significant increase of its total energy. This is displayed in Fig. 1.6 which shows the evolution of the adaptively chosen time increments and the total energy.

Acknowledgements Both authors acknowledge support by the German National Science Foundation DFG within the DFG Priority Program SPP 1253 'Optimierung mit partiellen Differentialgleichungen'. The first author has been further supported by the NSF grants DMS-0707602, DMS-0914788, by the BMBF within the projects 'FROPT' and 'MeFreSim', and by the ESF within the Networking Programme 'OPTPDE'.

References

1. Abkarian M, Lartigue C, Viallat A (2002) Tank treading and unbinding of deformable vesicles in shear flow: determination of the lift force. Phys Rev Lett 88(6):068103
2. Anadere I, Chmiel H, Hess H, Thurston GB (1979) Clinical blood rheology. Biorheology 16(3):171–178
3. Boffi D, Gastaldi L (2003) A finite element approach for the immersed boundary method. Comput Struct 81(8–11):491–501
4. Boffi D, Gastaldi L, Heltai L (2007) Numerical stability of the finite element immersed boundary method. Math Models Methods Appl Sci 17(10):1479–1505
5. Brezzi F, Fortin M (1991) Mixed and hybrid finite element methods. Springer, New York
6. Chien S (1970) Shear dependence of effective cell volume as a determinant of blood viscosity. Science 168:977–979
7. Chien S (1987) Red cell deformability and its relevance to blood flow. Annu Rev Physiol 49:177–192
8. Chmiel H, Anadere I, Walitza E (1990) The determination of blood viscoelasticity in clinical hemorheology. Clinical Hemorheology 10:363–374
9. Cokelet GR (1980) Rheology and hemodynamics. Annu Rev Physiol 42:311–324
10. Deuflhard P (2004) Newton methods for nonlinear problems. Affine invariance and adaptive algorithms. Springer, Berlin
11. Eggleton CD, Popel AS (1998) Large deformation of red blood cell ghosts in simple shear flow. Phys Fluids 10:1834–1845
12. Fischer T, Schmid-Schönbein H (1977) Tank treading motion of red blood cell membranes in viscometric flow: behavior of intracellular and extracellular markers. Blood Cells 3:351–365
13. Fischer TM, Stöhr-Liesen M, Schmid-Schönbein H (1978) The red cell as a fluid droplet—tank-treading like motion of the human erythrocyte membrane in shear flow. Science 202:894–896
14. Franke T, Hoppe RHW, Linsenmann C, Schmid L, Willbold C, Wixforth A (2011) Numerical simulation of the motion and deformation of red blood cells and vesicles in microfluidic flows. Comput Vis Sci 14(4):167–180
15. Hoppe RHW, Linsenmann C (2011) An adaptive Newton continuation strategy for the fully implicit finite element immersed boundary method. Submitted to J Comp Phys
16. Kantsler V, Steinberg V (2005) Orientation and dynamics of a vesicle in tank-treading motion in shear flow. Phys Rev Lett 95:258101
17. Keller SR, Skalak R (1982) Motion of a tank-treading ellipsoidal particle in a shear flow. J Fluid Mech 120:27–47
18. Le DV, White J, Peraire J, Lim KM, Khoo BC (2009) An implicit immersed boundary method for three-dimensional fluid-membrane interactions. J Comput Phys 228(22):8427–8445
19. Lee P, Griffith BE, Peskin CS (2010) The immersed boundary method for advection-electrodiffusion with implicit timestepping and local mesh refinement. J Comput Phys 229(13):5208–5227
20. Mori Y, Peskin CS (2008) Implicit second-order immersed boundary methods with boundary mass. Comput Methods Appl Mech Eng 197(25–28):2049–2067
21. Newren EP, Fogelson AL, Guy RD, Kirby RM (2007) Unconditionally stable discretizations of the immersed boundary equations. J Comp Physiol 222(2):702–719
22. Noguchi H, Gompper G (2004) Fluid vesicles with viscous membranes in shear flow. Phys Rev Lett 93:258102
23. Pan T-W, Wang T (2009) Dynamical simulation of red blood cell rheology in microvessels. Int J Numer Anal Model 6(3):455–473
24. Peskin CS (1977) Numerical analysis of blood flow in the heart. J Comput Phys 25(3):220–252
25. Peskin CS (2002) The immersed boundary method. Acta Numer 11:479–517
26. Pozrikidis C (2003) Modeling and simulation of capsules and biological cells. Chapman & Hall/CRC, Boca Raton

27. Pozrikidis C (2005) Axisymmetric motion of a file of red blood cells through capillaries. Phys Fluids 17(3):031503
28. Stockie JM, Wetton BR (1999) Analysis of stiffness in the immersed boundary method and implications for time-stepping schemes. J Comput Phys 154(1):41–64
29. Tartar L (2007) An introduction to Sobolev spaces and interpolation spaces. Springer, Berlin
30. Thurston GB (1972) Viscoelasticity of human blood. Biophys J 12(9):1205–1217
31. Thurston GB (1996) Viscoelastic properties of blood and blood analogs. In: How TV (ed) Advances in hemodynamics and hemorheology. JAI Press, London, pp 1–30
32. Tu C, Peskin CS (1992) Stability and instability in the computation of flows with moving immersed boundaries: a comparison of three methods. SIAM J Sci Stat Comput 13(6):1361–1376
33. Wang T, Pan T-W, Xing ZW, Glowinski R (2009) Numerical simulation of red blood cell rouleaus in microchannels. Phys Rev E 79(4):041916-1